PHYSICAL REVIEW C **85**, 054904 (2012)

Probing of compact baryonic configurations in nuclei in $A(p, \bar{p})X$ reactions and antiproton formation length in nuclear matter

Yu. T. Kiselev,[1,*] V. A. Sheinkman,[1] A. V. Akindinov,[1] M. M. Chumakov,[1] A. N. Martemyanov,[1] V. A. Smirnitsky,[1] Yu. V. Terekhov,[1] and E. Ya. Paryev[2]

[1]*Institute for Theoretical and Experimental Physics, Moscow 117218, Russia*
[2]*Institute for Nuclear Research, Russian Academy of Sciences, Moscow 117312, Russia*

(Received 3 November 2011; published 3 May 2012)

Inclusive cross sections $\sigma^A = Ed^3\sigma(X, P_t^2)/d^3p$ of antiproton and negative pion production on Be, Al, Cu, and Ta targets hit by 10-GeV protons were measured at the laboratory angles of 10.5° and 59°. Antiproton cross sections were obtained in both kinematically allowed and kinematically forbidden regions for antiproton production on a free nucleon. The antiproton cross-section ratio as a function of the longitudinal variable X exhibits three separate plateaus, which gives evidence for the existence of compact baryon configurations in nuclei—small-distance scaled objects of nuclear structure. The comparability of the measured cross-section ratios with those obtained in the inclusive electron scattering off nuclei suggests weak antiproton absorption in nuclei. Observed behavior of the cross-section ratios is interpreted in the framework of a model considering the hadron production as a fragmentation of quarks (antiquarks) into hadrons. It has been established that the antiproton formation length in nuclear matter can reach the magnitude of 4.5 fm.

DOI: 10.1103/PhysRevC.85.054904 PACS number(s): 25.40.Ve, 14.20.Dh, 21.65.−f, 25.70.−z

I. INTRODUCTION

The normal nuclear density of 0.16–0.17 nucleon/fm^3 corresponds to the average inter-nucleon (center-to-center) distance of 1.8–2 fm. Comparing this value with the electromagnetic radius of a proton $r_{\rm em} = 0.83$ fm shows that nucleons are tightly packed inside nuclei and almost overlap. Owing to quantum fluctuations of nuclear density, two or more nucleons can get even closer, forming dense cold compact baryonic configurations (CBCs). Current estimates of CBC size vary from 0.65 to 1 fm [1–3], which corresponds to a density about four- to eightfold the normal nuclear density. These values are comparable with those expected in the cores of neutron stars. In conventional nucleon-meson nuclear physics, CBCs are described as collections of closely packed nucleons usually referred to as short-range correlations (SRCs) of nucleons [4]. This description results in a universal shape of the nuclear wave function for all nuclei at $k > k_F$, where $k_F \sim 250$ MeV/c is the Fermi momentum of the nucleon [5]. However, one can expect that the densities of CBCs are high enough to modify the structure of underlying nucleon constituents. At short internucleon distances, nucleons can lose their identities and form multiquark configurations [3,6,7] or multinucleon quark clusters [8]. Studying CBCs provides information on the features of the nuclear structure at small-distance scales as well as on the equation of state of a cold and dense matter.

High-energy lepton scattering on nuclei is an effective method of probing CBCs. In deep inelastic physics, cross sections are typically plotted as functions of the Bjorken scaling variable $x_B = Q^2/2m\omega$, where Q is the four-momentum transferred to the system, ω is the energy transfer, and m is the mass of a proton. The value of x_B determines the fraction of the struck quark's momentum relative to the nucleon momentum in the infinite momentum frame. Obviously, a constituent of an isolated nucleon carries $x_B \leqslant 1$. Both approaches, SRC [4] and quark clustering in nuclei [8], lead to a simple prediction for the region $x_B > 1$, where cooperative effects are required to provide scattering process. Regardless of the nucleon or quark content of the CBCs, the ratio of inclusive electron scattering cross sections for two different nuclei has a scaling behavior at high-momentum transfer and large x_B values, which depends only on the ratio of probabilities of finding CBCs in those two nuclei. This scaling manifests itself as a plateau in the ratio when it is plotted as a function of x_B. Such plateaus were first observed at the SLAC [9] and, subsequently, at the Jefferson Laboratory (JLab) [10,11]. In 1983, the European Muon Collaboration (EMC) measured the deep-inelastic per-nucleon cross-section ratio of ^{56}Fe over deuterium in a broad kinematic range [12]. The measured ratio revealed an unexpected structure which was subsequently confirmed by SLAC [13] and became known as the "EMC effect." Plotted as functions of the Bjorken scaling variable x_B, the ratios showed a clear decrease at $0.3 < x_B < 0.7$ and a sharp rise at $x_B > 0.8$. These results generated considerable experimental and theoretical interest, but none of the existing models has been able to explain the effect over the whole range of x_B and A. New high-precision experimental data on the EMC effect in light nuclei obtained at JLab [14] suggest that the slope in the $0.3 < x_B < 0.7$ region is an effect of local density and is not a bulk property of the nuclear medium. At similar four-momentum transfers, data of the HMS Collaboration (JLab) [11] indicated that the nuclear scaling plateaus at $x_B > 1$ also represent an effect of local density. The authors of Ref. [15] found a linear correlation between the strength of the EMC effect, defined as the slope of the cross-section ratios in the range $0.3 < x_B < 0.7$, and the nuclear scaling plateaus at $x_B > 1$. These results are consistent with the idea that both effects scale with the local nuclear environment.

*yurikis@itep.ru

Studying cumulative reactions provides complementary information on localized dense objects inside nuclei. Cumulative hadron production can be the key to understanding the process of hadron creation in the fragmentation region of a nucleus beyond the kinematical limits of the production of these hadrons in the collisions of elementary projectiles with isolated nucleons. In 1980–1990s cumulative hadron production was intensively investigated in many experiments using a variety of beam particles and energies. Proton-induced production of high-momentum cumulative protons, pions, kaons, antikaons, and antiprotons [2,16] has been studied up to the value of $X \sim 3.5$, where X is a variable similar to the Bjorken x_B (see Sec. III). The uncertainty principle requires that such hadrons could arise from fluctuations of dense CBCs consisting of either a few closely packed nucleons with a high relative momentum [4] or quark constituents of a multiquark configuration carrying a light cone momentum fraction greater than that of a single nucleon [3]. It is worth noting that the study of superfast quarks in deep inelastic scattering at $x_B > 1$ is one of the three key experimental programs of the future 12-GeV JLab facility [1]. In cumulative reactions, a nucleus acts both as a target and as an analyzer of the interaction of products with the nuclear environment. Therefore, the study of cumulative reactions provides information on the hadronization process in nuclear matter, a subject which is also of great current interest. Investigation of cumulative antiproton production in pA reactions is of special interest because the antiproton does not contain nuclear valence quarks. In this paper we report on the study of cumulative antiproton production off nuclei. Two experiments were performed using the internal 10-GeV beam of the ITEP proton synchrotron and nuclear targets. In the first experiment invariant cross sections were measured at 59° (lab) in the antiproton momentum interval of 0.6–1.7 GeV/c, which corresponds to the cumulative region. In the second experiment the data on cross sections were obtained at 10° (lab) in the momentum range allowed for antiproton production on free nucleons. Invariant cross sections of π^- meson production on the same set of nuclear targets were measured simultaneously. The goals of the experiments were to search for the presence of CBCs in nuclei as well as to study antiproton absorption in the nuclear matter.

II. EXPERIMENTAL ARRANGEMENT

Experiments were carried out with the internal proton beam of the 10-GeV ITEP synchrotron irradiating Be, Al, Cu, and Ta strip targets, 60–150 μm thick. Secondary particles produced at 10.5° and 59° (lab) in the momentum range from 0.6 to 2.5 GeV/c were detected by two identical arms of the focusing hadron spectrometer. Each arm was composed of two bending dipole magnets and two pairs of quadrupole magnets. The momentum and angular acceptance of the magnetic channels were $\Delta p/p = 1\%$ and 0.8 msr, correspondingly. Two multiwire proportional chambers located at the second focus of each magnetic system controlled the beam position during data collection. The particle identification system included a two-stage time-of-flight (TOF) system based on scintillation counters and two Cherenkov counters. TOF measurements were performed over two bases of 11 and 17 m. Two XP2020 photomultipliers (PMs) mounted on both sides of each scintillator provided the mean-time signal for TOF measurement and two energy loss (dE/dx) signals. The time resolution of the TOF system was less than 300 ps (FWHM). In the momentum range 0.6–1.3 GeV/c, the threshold Cherenkov counter with a water radiator was used for suppression of the pion background. Analysis of the information on dE/dx and TOF allowed selection of antiprotons in the above-mentioned momentum range. At higher $\bar{p}$ momenta, the trigger also included a signal from the differential Cherenkov counter. The counter optics was adjusted for detection of antiprotons with a given momentum selected by the magnetic system. Photons emitted by antiprotons in the radiator of the differential Cherenkov counter (glycerin-water mixture) were detected by a ring consisting of 12 PMs. The velocity resolution of the Cherenkov counter was $\Delta\beta/\beta = 2\%$. The antiproton selection criterion handled by hardware included a requirement that eight PMs of the ring were fired in a single event. For each event, information on a larger number of fired PMs (9 and 10) was also recorded. The identification reliability increased with the increasing number of operated PMs, leading, however, to a decrease in the detection efficiency. This efficiency varied from 35% to 75%, depending on the number of operated PMs and was periodically tested in special measurements using protons with the same velocity. Depending on the effect-to-background ratio, the information on different number of fired PMs was used during the off-line analysis. Selection of antiprotons was quite reliable down to the ratio of $\bar{p}/\pi^- = 10^{-6}$. The misidentification probability was less than 4% for almost all data and did not exceed 7% at the lowest cross-section value. Secondary antiprotons and pions were detected simultaneously. The measured antiproton and negative pion yields were corrected for the loss owing to nuclear interactions and multiple scattering in the material of the spectrometer, detector efficiencies, and pion in-flight decay at a distance of 32 m from the production target toward the second focus of the magnetic channels. In order to determine the absolute value of the pion differential cross sections on different nuclear targets, π^- yields at 10° and 59° were measured along with the flux of protons traversing the sandwich-type targets made of thin (12-μm) Al foil and Be, Al, Cu, or Ta strips used as the production targets. Determination of the incident proton flux was performed by measuring the induced γ activity in the reaction $p + {}^{27}\mathrm{Al} \rightarrow {}^{24}\mathrm{Na}^* + X$. Knowing the cross section of this reaction and the acceptance of the magnetic channels allowed calculation of the differential cross sections for π^- production at 10° and 59°. Pion cross sections were then used for absolute normalization of the differential cross sections for antiproton production, as the ratio of the antiproton yield to that of the pion was measured at each secondary momentum. The resulting uncertainty of the absolute normalization of the cross sections was estimated as 17% and 20% for data obtained at 10° and 59°, respectively. The measured invariant cross sections are reported in Tables I –IV. The errors quoted in these tables do not include uncertainties in the absolute normalization.

TABLE I. Invariant cross sections $\sigma^A = Ed^3\sigma/d^3p$ [GeV μb/(GeV/c)^3] of $\bar{p}$ production at a total energy of the incident proton of 10 GeV and at a laboratory angle of 10.5°. Statistical (first) and systematical (second) errors are presented. Systematic errors include the correction uncertainties and reproducibility of measurements.

p (GeV/c)	Be	Al	Cu	Ta
0.73	6.48 ± 0.32 ± 0.8	18.1 ± 0.9 ± 2.2	28.3 ± 1.4 ± 3.4	42.6 ± 2.1 ± 5.1
0.93	11.6 ± 0.46 ± 1.2	31.1 ± 1.2 ± 3.1	45.0 ± 1.8 ± 4.5	58.8 ± 2.4 ± 5.9
1.31	23.0 ± 0.98 ± 2.5	61 ± 2.6 ± 6.5	91.1 ± 3.9 ± 9.7	141 ± 6 ± 15
1.76	19.3 ± 0.78 ± 1.5	46.7 ± 1.9 ± 3.7	66.6 ± 2.7 ± 5.3	111 ± 4.4 ± 8.9
2.47	8.51 ± 0.34 ± 0.7	20.4 ± 0.82 ± 1.6	27.7 ± 1.1 ± 2.2	47.3 ± 1.9 ± 3.8

III. RESULTS AND DISCUSSION

Measured in the experiment were the invariant inclusive cross sections $\sigma^A = Ed^3\sigma(X, P_t^2)/d^3p$ of antiproton production on target nucleus with atomic number A. The transverse variable P_t^2 was derived from the absolute value of antiproton momentum and from its production angle. To determine the longitudinal variable X we used the minimal mass of the intranuclear target, expressed in units of nucleon mass m, for which the production of an antiproton with registered three-momentum was kinematically possible. The variable X is called a cumulative number. It can be obtained from Eq. (1), expressing conservation of the energy-momentum and baryonic number in the reaction $p + mX \to \bar{p} + \cdots$:

$$(\hat{P}_0 + m\hat{X} - \hat{P})^2 \geqslant [(2+X)m]^2, \quad (1)$$

where $\hat{P}_0$, $\hat{P}$, and $m\hat{X}(mX, \mathbf{0})$ are the four-momenta of the incident proton, detected antiproton, and intranuclear target, respectively. By equating the left- and right-hand sides of Eq. (1), one obtains

$$X = \left(1 - \frac{E}{E_0} - \frac{2m}{E_0}\right)^{-1} \left(\frac{E - \beta_0 P\cos\theta}{m} + \frac{m}{E_0}\right), \quad (2)$$

where E_0 and P_0 are the total energy and three-momentum of the projectile proton, $\beta_0 = P_0/E_0$; E, P, and θ are the total energy, three-momentum, and antiproton production angle in the laboratory system, respectively. The value $X = 1$ corresponds to the kinematical limit of antiproton creation on a nucleon at rest, while in the cumulative region $X > 1$. The definition of X [Eq. (2)] takes into account the finite energy E_0 of the projectile proton. As the energy E_0 increases, X tends to the light cone variable $\alpha = (E - P_l)/m$. Note that the Bjorken variable x_B can also be interpreted as the minimum target mass in the nucleon mass units, i.e., the variable expressing the number of nucleons involved in the deep inelastic scattering process. The invariant inclusive cross section of antiproton production on the nucleus can be represented in a form similar to that used in Ref. [10] for the description of inclusive electron scattering on nuclei:

$$\sigma^A\left(X, P_t^2\right) = A\sum_{j=1}^{A} \frac{W_j^A}{j}\sigma_j\left(X, P_t^2\right) f_{\text{FSI}}^A \theta(j - X), \quad (3)$$

$$\sum_{j=1}^{A} W_j^A = 1. \quad (4)$$

Here, $W_j^A = m_j/A$ is the per-nucleon probability that m_j nucleons of the target nucleus with mass number A belong to CBCs with a given j, f_{FSI}^A stands for a factor describing the absorption of the outgoing antiproton on its way out of the nucleus (FSI, final-state interaction), and $\theta(x)$ is the step function. Depending on the model of cumulative hadron production, $\sigma_j(X, P_t^2)$ can be considered either as a cross section of the proton-j-nucleon correlation [4] or as a cross section of a proton interaction with a colorless configuration consisting of j $3q$ systems [3]. Equation (3) does not take into account the initial-state interaction of the projectile proton for a reason discussed later in this section. Because the probabilities W_j^A have to drop rapidly with j, one may expect that interactions with j-CBC will dominate in the region $j - 1 < X < j$. Therefore, the ratio of nuclear antiproton production cross sections to nucleons of heavy A_1 and light A_2 nuclei in this region has to be independent of the cross section $\sigma_j(X, P_t^2)$ and have discrete values for different j:

$$R_j = \frac{A_2}{A_1}\frac{\sigma^{A_1}}{\sigma^{A_2}} = \frac{W_j^{A_1}}{W_j^{A_2}}\frac{f_{\text{FSI}}^{A_1}}{f_{\text{FSI}}^{A_2}}. \quad (5)$$

Because the ratio $\frac{W_j^{A_1}}{W_j^{A_2}}$ has to increase with A and j, one can expect that discrete values of R_j would also exhibit a similar behavior provided that the ratios of the absorption factors $\frac{f_{\text{FSI}}^{A_1}}{f_{\text{FSI}}^{A_2}}$ are almost constant at each j.

The experimental data on inclusive electron scattering cross sections on nuclei ^{3}He, ^{4}He, ^{12}C, and ^{56}Fe obtained by the CLAS Collaboration (JLab) [10] at the four-momentum transfer to the target $1.4 < Q^2 < 2.6$ (GeV/c)^2 and at the

TABLE II. Invariant cross sections $\sigma^A = Ed^3\sigma/d^3p$ [GeV mb/(GeV/c)^3] of π^- production at a total energy of the incident proton of 10 GeV and at a laboratory angle of 10.5°. Statistical errors are negligible. The systematic error of each cross section equals 8% and includes the uncertainties of the corrections and reproducibility of measurements.

p (GeV/c)	Be	Al	Cu	Ta
0.73	300	762	1214	2198
0.93	194	483	736	1286
1.31	96.8	233	351	603
1.76	45.6	108	160	268
2.47	15.8	36.7	53.1	88.7

TABLE III. Invariant cross sections $\sigma^A = Ed^3\sigma/d^3p$ [GeV nb/(GeV/c)^3] of $\bar{p}$ production at a total energy of the incident proton of 1 GeV and at a laboratory angle of 59°. Statistical (first) and systematical (second) errors are presented. Systematic errors include the correction uncertainties and reproducibility of measurements.

p (GeV/c)	Be	Al	Cu	Ta
0.58	61 ± 4 ± 7	216 ± 15 ± 26	472 ± 33 ± 57	634 ± 44 ± 76
0.69	82 ± 5 ± 9	367 ± 22 ± 40	718 ± 43 ± 79	1129 ± 68 ± 124
0.78	78 ± 5 ± 8	329 ± 20 ± 33	614 ± 37 ± 61	967 ± 58 ± 97
0.88	79 ± 5 ± 8	331 ± 20 ± 33	681 ± 41 ± 68	938 ± 56 ± 94
0.98	51 ± 3 ± 5	260 ± 13 ± 26	408 ± 20 ± 41	744 ± 37 ± 74
1.07	38.1 ± 1.5 ± 3.8	178 ± 7 ± 18	234 ± 9 ± 23	456 ± 22 ± 46
1.19	14.0 ± 0.6 ± 1.3	85 ± 3 ± 8	172 ± 7 ± 15	299 ± 14 ± 27
1.35	5.7 ± 0.3 ± 0.5	32 ± 2 ± 3	79 ± 5 ± 6	140 ± 10 ± 11
1.53	1.4 ± 0.14 ± 0.11	11.6 ± 1.2 ± 0.9	28 ± 2.8 ± 2.2	40 ± 4 ± 4
1.72	0.3 ± 0.04 ± 0.02	2.5 ± 0.35 ± 0.2	5.1 ± 0.7 ± 0.4	

Bjorken variable $1 < x_B < 2.8$ indicate the existence of such regions. Cross-section ratios $R = (3\sigma^A)/(A\sigma^{^3\mathrm{He}})$ exhibit two separate plateaus, at $1.5 < x_B < 2$ and at $x_B > 2.25$, interpreted by the authors of Ref. [10] as evidence for the presence of compact two- and three-nucleon SRCs in nuclei. Similar behavior of cross-section ratios was observed later by the HMS Collaboration at JLab [11].

In the subsequent analysis, along with the cross sections measured in the present experiment at the laboratory angles of 10° and 59°, we also use data on cumulative antiproton production by 10-GeV protons obtained on the same set of target nuclei at the laboratory angles of 97° and 119° which were presented in our previous work [16]. The X dependence of the ratio $R_j(X)$ in the region $0.53 < X < 2.83$ is shown in Fig. 1.

To analyze the behavior of $R_j(X)$ in more detail, the measured ratios $R_j = (9\sigma^{\mathrm{Al}})/(27\sigma^{\mathrm{Be}}) = R_j(\mathrm{Al/Be})$ and $R_j = (9\sigma^{\mathrm{Ta}})/(181\sigma^{\mathrm{Be}}) = R_j(\mathrm{Ta/Be})$ were multiplied by factors chosen in such a way that their average values were equalized with the average magnitude of the ratio $R_j = (9\sigma^{\mathrm{Cu}})/(64\sigma^{\mathrm{Be}}) = R_j(\mathrm{Cu/Be})$. The first plateau is clearly seen at $0.5 < X < 0.85$; the second plateau, at $1.3 < X < 1.6$. The ratio increases with X, which is related to the contribution of CBCs with $j = 3$. Figure 1 also demonstrates the presence of a third plateau in the region $1.8 < X < 2.4$. The observed increase in the cross-section ratio at $X > 2.5$ can be explained as a transition from a CBC with $j = 3$ to a CBC with $j = 4$.

Note that the absolute values of antiproton production cross sections in the plateau regions vary by several orders of magnitude. The plotted cross-section ratios correspond to different antiproton momenta and production angles and, hence, to different values of the transverse momenta P_t^2 varying from 0.3 to 2 (GeV/c)^2. Therefore, the ratios $R_j(A/\mathrm{Be})$ exhibit the scaling behavior on each plateau ($j = 1, 2, 3$); i.e., they do not depend on X or on P_t^2. Similar behavior of the cross-section ratios (independence from x_B and Q^2) was observed in JLab experiments [10,11]. It should be noted that the plateaus which correspond to $j = 2, 3$ in the JLab results [10,11] were observed at values of x_B larger than the values of X obtained in our experiment. The main reason for this apparent discrepancy is the use of different variables: X is similar but not equivalent to x_B. Besides, as discussed later in this section, there is a physical reason for the downward shift of the plateaus in reactions with detection of a hadron in the final state compared to inclusive electron scattering reactions.

The cross-section ratios can be determined more precisely than the absolute values of cross sections, as the detector-dependent errors, many of the correction factors, and most

TABLE IV. Invariant cross sections $\sigma^A = Ed^3\sigma/d^3p$ [GeV mb/(GeV/c)^3] of π^- production at a total energy of the incident proton of 10 GeV and at a laboratory angle of 59°. Statistical errors are negligible. The systematic error of each cross section is 8% and includes the uncertainties of the corrections and reproducibility of measurements.

p (GeV/c)	Be	Al	Cu	Ta
0.58	20.3	59.3	121	226
0.69	12.6	36.7	70	134
0.78	7.03	21.6	43.8	79.6
0.88	4.02	11.6	24.1	45.3
0.98	1.81	5.92	12.1	23.5
1.07	0.87	3.03	6.33	12.2
1.19	0.332	1.25	2.85	5.43
1.35	8.21×10^{-2}	0.43	0.922	1.81
1.53	2.04×10^{-2}	0.114	0.271	0.542
1.72	3.02×10^{-3}	1.96×10^{-2}	4.97×10^{-2}	1.13×10^{-1}

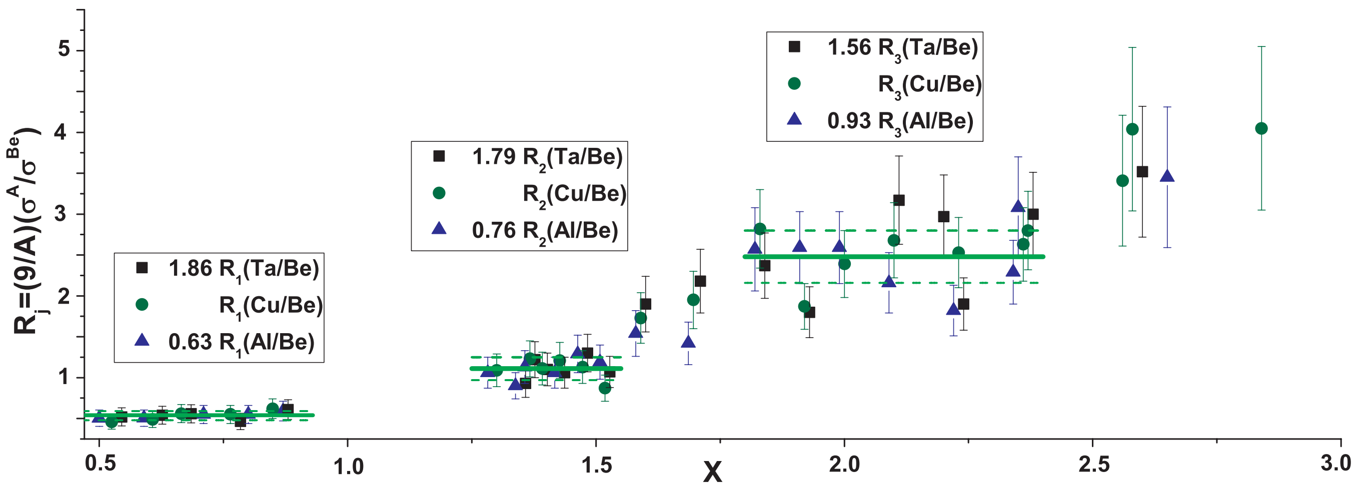

FIG. 1. (Color online) Cross-section ratio $R = (9\sigma_{pA\to\bar{p}})/(A\sigma_{p\mathrm{Be}\to\bar{p}})$ as a function of X in the range $0.5 < X < 2.8$. Values of the rescaling factors for $j = 1, 2, 3$ are indicated in the legends from left to right, respectively. Solid and dashed lines correspond to the weighted-average magnitudes of R(Cu/Be) and their errors listed in Table V. Symbols for Al/Be and Ta/Be ratios are slightly displaced.

of the absolute normalization uncertainty cancel out in the ratios. As a result, the error of each individual value of the cross-section ratio $R_j(A/\mathrm{Be})$ shown in Fig. 1 contains only a residual of the systematic error. The error bars manifest the statistical and remaining systematic errors added in quadrature. The weighted-average magnitudes of $R_j(A/\mathrm{Be})$ are presented in Table V.

As seen from Eq. (5), the values of $R_j(A/\mathrm{Be})$ depend on the probabilities W_j^A. These probabilities were calculated within a model identifying CBCs with SRCs [4], and within a model considering CBCs as quark clusters [8]. Calculations of the probabilities W_j^A for $j = 2, 3$ in Ref. [4] are based on the analysis of hadron production on light nuclei and on the Fermi liquid theory of ^{56}Fe. According to the model [8], two nucleons form a six-quark cluster when they are separated by less than a critical distance $d_c = 2R_c = 1$ fm, where R_c is a nucleon critical "color percolation" radius. A third nucleon, distanced less than d_c from the first two, may join the cluster to form a nine-quark cluster, etc. In both approaches, the calculation results are model- dependent. Because the values of W_j^A for $j = 2, 3$ obtained in the model [4] have essentially weaker A and j dependencies compared to those calculated in Ref. [17] within the model [8], the absolute values of W_2^A and W_3^A in these models differ significantly (see discussion in Ref. [10]). However, the probability ratios W_j^A/W_j^{Be}, entering Eq. (5), almost do not depend on the chosen model. For example, the difference in the magnitudes of ratios $W_2^{\mathrm{Fe}}/W_2^{\mathrm{C}}$ and $W_3^{\mathrm{Fe}}/W_3^{\mathrm{C}}$ from Refs. [4,17] does not exceed 5%. The probabilities W_j^A were calculated in Ref. [4] for light nuclei and for the iron nucleus ($A = 56$), whereas in Ref. [17] they were obtained on the same footing for a wide range of nuclei, from helium to uranium. Therefore, in the subsequent analysis we use the probability ratios presented in Table VI, W_j^A/W_j^{Be} ($j = 1, 2, 3$) calculated in Ref. [17] within the quark-cluster model [8].

Comparing the measured ratios $R_j(\mathrm{Al/Be})$ (first row in Table V) to the ratios $W_j^{\mathrm{Al}}/W_j^{\mathrm{Be}}$ (first row in Table VI), one can see that the ratio of the absorption factors $f_{\mathrm{FSI}}^{\mathrm{Al}}/f_{\mathrm{FSI}}^{\mathrm{Be}}$ in Eq. (5) is close to 1 for all j. This suggests weak absorption of antiprotons in light nuclei, up to Al. The lower values of the cross-section ratios listed in the second and third rows in Table V, compared to the probability ratios presented in the corresponding rows in Table VI, indicate the presence of antiproton absorption in intermediate and heavy nuclei.

Figure 2 shows the A dependence of the antiproton production cross-section ratios $\tilde{R}_j(A/\mathrm{Be}) = R_j(A/\mathrm{Be})(A/9)$ for various j. The points correspond to the ratios $R_j(A/\mathrm{Be})$ listed in Table V, and they are linked by lines to guide the eyes. One can see that this dependence becomes steeper with an increase in X. The main reason for this change in A dependence is the fast growth of the ratios W_j^A/W_j^{Be} with j. Despite the fact that the experimental dependencies do not follow well the simple one-parameter power-law dependence $\sigma^A = \sigma_0 A^\alpha$, we calculate the exponent α to characterize its change with j. The exponent α, calculated taking into account antiproton creation cross sections on all nuclei in the region where CBCs

TABLE V. Cross-section ratio $R_j = (9\sigma_{pA\to\bar{p}})/(A\sigma_{p\mathrm{Be}\to\bar{p}})$ for $j = 1, 2, 3$.

R_j	$j = 1$ $(0 \leqslant X \leqslant 1)$	$j = 2$ $(1 \leqslant X \leqslant 2)$	$j = 3$ $(2 \leqslant X \leqslant 3)$
Al/Be	0.86 ± 0.08	1.45 ± 0.12	2.77 ± 0.25
Cu/Be	0.54 ± 0.05	1.11 ± 0.09	2.48 ± 0.22
Ta/Be	0.29 ± 0.03	0.63 ± 0.05	1.74 ± 0.20

TABLE VI. Probability ratios W_j^A/W_j^{Be} calculated based on data from Table IV [17].

W_j^A/W_j^{Be}	$j = 1$	$j = 2$	$j = 3$
Al/Be	0.92	1.65	2.8
Cu/Be	0.90	1.80	3.4
Ta/Be	0.88	1.86	3.6

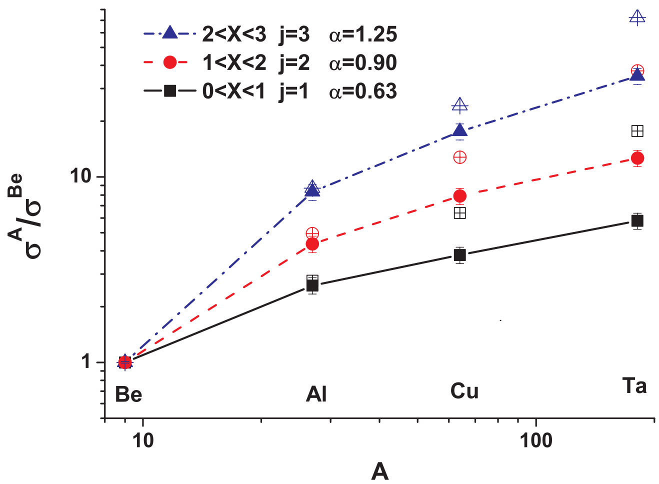

FIG. 2. (Color online) A dependence of the cross-section ratio $\sigma^A/\sigma^{\mathrm{Be}}$ for $j = 1, 2, 3$. Filled symbols are data points. Values of exponent α from the power-law approximation of the measured ratio $(A/9)^\alpha$ are indicated in the legend. Magnitudes of the cross-section ratio calculated using the data in Table VI are shown by open symbols with crosses.

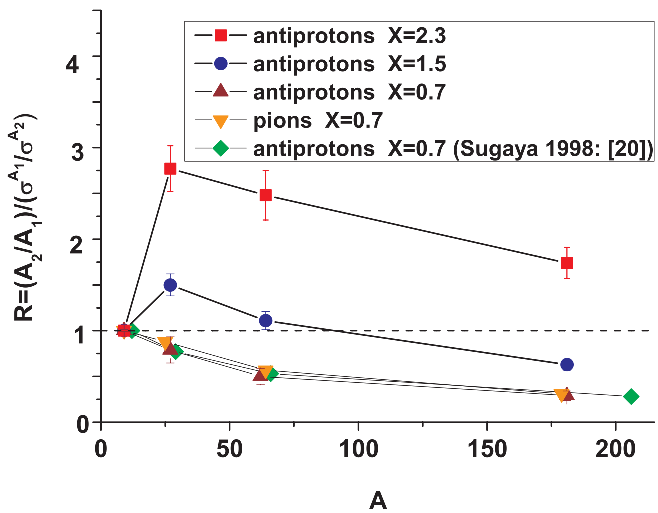

FIG. 3. (Color online) Atomic mass dependence of the transparency ratio R for antiprotons and pions in the cumulative ($X > 1$) and noncumulative ($X \leqslant 1$) regions.

with $j = 3$ dominate antiproton production, exceeds 1 and is approximately equal to 1.25.[1] The experimental value of the ratio $\tilde{R}_3(\mathrm{Al/Be}) = 8.3$ corresponds to $\alpha = 1.9 \pm 0.1$, which is in good agreement with the magnitude $\alpha = 1.94$, obtained using the ratio $W_3^{\mathrm{Al}}/W_3^{\mathrm{Be}} = 2.8$ from Table VI.

The per-nucleon cross-section ratio $R = (\sigma^{A_1}/A_1)/(\sigma^{A_2}/A_2)$ [Eq. (5)] is often referred to as the transparency ratio. It is widely believed that the target mass dependence of R is determined by the attenuation of the flux of produced particles in the nuclei, which, in turn, is governed by its in-medium width Γ (see review in Ref. [19]).

Figure 3 demonstrates that the A dependencies of the ratio R, given in Table V, in noncumulative ($X \leqslant 1$) and in cumulative ($X > 1$) regions are substantially different. In the noncumulative region, the ratio R, normalized to the cross section on a light nucleus, is always less than 1 and it decreases as A increases for all species of secondary particles. The respective ratios of the antiproton and π^--meson production cross sections measured in the present experiment in the same region, as well as the corresponding ratios of the cross sections for antiproton creation on C, Cu, and Pb nuclei by 12-GeV protons from Ref. [20], follow the same dependence. The measured transparency ratios for ϕ mesons in photon-induced [21] and proton-induced reactions [22], as well as for photoproduced ω mesons [23], behave in the same way. In the cumulative region, R behaves in an essentially different way. The values of $R(A)$ significantly exceed 1 and go up to ~2.5. It must be emphasized that the transparency ratio R is determined not only by the absorption of the produced hadrons but also by the mechanism of their production. In the kinematically allowed region $0 \leqslant X \leqslant 1$, the ratios $W_1^{\mathrm{A}}/W_1^{\mathrm{Be}}$ depend weakly on A and are close to 1 (column $j = 1$ in Table VI). In this case the ratio R is mainly governed by the ratio of absorption factors. In the cumulative region $X > 1$, the ratios $W_j^{\mathrm{A}}/W_j^{\mathrm{Be}}$ (columns $j = 2$ and $j = 3$ in Table VI) significantly exceed 1 and therefore the values of R depend on these two factors.

Direct comparison of the cross-section ratios measured in the $A(p, \bar{p})$ and $A(e, e')$ reactions is hindered by the use of different targets. The ratios measured in our experiment are $R_2(^{64}\mathrm{Cu}/^9\mathrm{Be}) = 1.11 \pm 0.09$ and $R_3(^{64}\mathrm{Cu}/^9\mathrm{Be}) = 2.48 \pm 0.22$, whereas in Ref. [10] $R_2(^{56}\mathrm{Fe}/^{12}\mathrm{C}) = 1.17 \pm 0.12$ and $R_3(^{56}\mathrm{Fe}/^{12}\mathrm{C}) = 1.44 \pm 0.18$.[2] However, reasonable comparison can be performed provided that the difference in the ratio of probabilities $W_j^{A_1}/W_j^{A_2}$ is taken into account. According to Ref. [17], the values of W_j^{Cu} and W_j^{Fe} (for $j = 2, 3$) are almost the same, while the ratio $W_2^{\mathrm{C}}/W_2^{\mathrm{Be}} = 1.5$ and $W_3^{\mathrm{C}}/W_3^{\mathrm{Be}} = 2.4$ with a theoretical uncertainty of 10%. Because $W_j^{\mathrm{Cu}}/W_j^{\mathrm{Be}} = (W_j^{\mathrm{Fe}}/W_j^{\mathrm{C}})(W_j^{\mathrm{C}}/W_j^{\mathrm{Be}})$, the values expected for inclusive electron scattering are $R_2(^{64}\mathrm{Cu}/^9\mathrm{Be}) = 1.76 \pm 0.25$ and $R_3(^{64}\mathrm{Cu}/^9\mathrm{Be}) = 3.46 \pm 0.55$. These values are in good agreement with the values of 1.8 and 3.4 in Table VI. The value $R_2(^{64}\mathrm{Cu}/^9\mathrm{Be}) = 1.32 \pm 0.15$,[3] measured by the HMS Collaboration at $Q^2 = 3.73$ GeV^2 [11], falls between $R_2(^{64}\mathrm{Cu}/^9\mathrm{Be}) = 1.11 \pm 0.09$ (obtained in our experiment) and 1.76 ± 0.25 (the expected magnitude cited above). Therefore, the values $R_j(A/\mathrm{Be})$ from the present experiment are comparable to, but still less than, those extracted from the data on inclusive electron scattering off nuclei [10,11]. This difference should be attributed to the antiproton absorption in

[1]Similar values of $\alpha > 1$ were observed for antiproton production on nuclei with a high transverse momentum ("Cronin effect") [18]. In both cases, nucleons behave cooperatively.

[2]Statistical and systematic errors quoted in Ref. [10] have been added in quadrature.

[3]Statistical and systematic errors quoted in Ref. [11] have been added in quadrature. Unfortunately, the HMS data in the range of $j = 3$ suffer from poor statistics, which makes numerical comparison with our experimental results difficult.

intermediate and heavier nuclei. If antiprotons are not absorbed in nuclei, the ratio $f_{\rm FSI}^{A}/f_{\rm FSI}^{\rm Be} = 1$. In this case the ratios $\tilde{R}_j(A/{\rm Be}) = R_j(A/{\rm Be})(A/9)$, shown in Fig. 2 by the open symbols containing crosses, are defined by the probability ratios from Table VI. The difference between filled and open symbols characterizes the magnitude of the effect of antiproton absorption in different nuclei.

Our estimate of the antiproton absorption in nuclei is inspired by the quark gluon string model based on $1/N$ expansion in QCD [3], as well as by the three-stage model of hadron formation in nuclear medium [24–26]. The model [3] presumes the existence of CBCs as an inherent property of the nuclear structure and considers the process of cumulative hadron production $pA \to hX$ in the reference frame where the nucleus moves with a high momentum. This consideration is equivalent to the analysis in the rest frame of the target nucleus. It is assumed that this nucleus is composed of the usual nucleons with a probability W_1^A and of $3j$-quark colorless CBCs with a probability W_j^A, where j changes from 2 to A. According to the model, each CBC initially contains a quark configuration of the X and P_t distribution. The value X determines a fraction of the quark momentum relative to the CBC momentum in the rest frame of the moving nucleus. Interaction of the moving nucleus with the target results in the production of hadrons in the fragmentation range of nucleus A. Cumulative hadrons with $X > 1$ originate from the quark (antiquark) fragmentation of a massive $3j$ ($j > 1$) CBC into hadrons (antiprotons in our case). This model allows quantitative description of the cross sections and some specific features of the cumulative hadron production [3]. Processes in the fragmentation regions of the nucleus and the target become independent at high collision energies. Indeed, experimentally observed shapes of the cumulative hadron distributions are insensitive to the types of beam particles. This fact, together with the observed comparability of the cross-section ratios measured in the $A(p, \bar{p})$ and $A(e, e')$ reactions, supports the idea that the properties of the target (proton or electron) are not essential for analysis of the cross-section ratios. Therefore, Eqs. (3) and (5) do not include the initial-state interaction of the incident proton with the nuclear matter, and the ratio R depends only on the FSI of the produced antiproton. Some models [24–26] consider hadron formation in semi-inclusive deep inelastic scattering on nuclei as a three-step process. During the first (production) stage, the quark (antiquark) propagates quasifreely, undergoing multiple collisions with nucleons. During the second (formation) stage, color neutralization takes place and a small colorless prehadron is created that has a reduced absorption cross section; subsequently the hadron wave function is formed. During the third (propagation) stage, the surviving prehadron transforms into the final-state (detected) hadron. Absorption of the hadron on its way out of the nucleus is governed by the "normal" hadron-nucleon cross section.

To estimate the antiproton formation length in the nuclear matter, we use a simplified two-stage model. Our analysis does not make a distinction between the production length and the formation length, dealing with the total effect referred to as the "formation length." During the first (formation) stage, a quark (antiquark) ejected from the CBC at some point O_1 inside the nucleus propagates without interaction with the nuclear environment until the hadronic antiproton emerges at point O_2. The antiproton formation length L in the nucleus rest frame is defined as the distance traveled by the quark between point O_1 and point O_2. During the second (propagation) stage, the antiproton travels farther in the same direction before escaping the nucleus. Interactions of the antiproton with nucleons on its way out of the nucleus are determined by the momentum-dependent total cross section $\sigma_{\bar{p}N}^{\rm tot}(P_{\bar{p}})$ in the free space [27].

We evaluated the length L using the following procedure. The left-hand side of Eq. (5) was determined as the ratio R of the measured cross sections for each specific antiproton momentum and production angle. The ratios $W_j^{A_1}/W_j^{A_2}$, entering the right-hand side of Eq. (5), were taken from Table VI. The ratio $f_{\rm FSI}^{A}/f_{\rm FSI}^{\rm Be}$ depends on L and characterizes the propagation stage of a formed antiproton in the nucleus. This ratio was calculated within the Glauber model, accounting for the actual nucleon densities and arbitrary antiproton production angles. Subsequently we treated L as a free parameter and determined the value of L as satisfying Eq. (5). We estimated L using the cross-section ratios measured in the range of dominance of CBCs with $j = 3$. Calculation of the antiproton production length using the ratio $R_3({\rm Al/Be})$ gave $L \geqslant (2 \div 3) r_{\rm Al}$, where $r_{\rm Al}$ is the radius of the Al nucleus. As noted above, this indicates that the absorption of antiprotons in light nuclei is weak. The values of L, obtained from the experimental data on the cross-section ratios $R_3({\rm Cu/Be})$ and $R_3({\rm Ta/Be})$, are listed in Table VII.

The data presented in Table VII show that the formation length L does not depend (within the uncertainties) either on the momentum or on the antiproton production angle and is governed only by the properties of CBCs with $j = 3$. The weighted-average value of L, calculated using data from Table VII, equals $4.5^{+0.5}_{-0.7}$ fm. This number is comparable to the radii of an intermediate nuclei with $A \approx 60$ ($R_{1/2}^{\rm Cu} = 4.2$ fm). Similar calculations, employing the ratios $R_2(A/{\rm Be})$ ($A =$ Cu, Ta) measured in the region where CBCs with $j = 2$ dominate, lead to $L = 2.8^{+0.6}_{-0.7}$ fm. In the region where CBCs with $j = 1$ dominate, $L = 2.0^{+0.6}_{-0.8}$ fm, this value being comparable to the average separation of nucleons inside a nucleus of $1.8 \div 2$ fm.

The observed increase in L with j is in agreement with predictions of the three-step model [24–26]. According to the model, the hadron formation length L in the nuclear rest frame is proportional to the energy of the initial quark. Indeed, the energy of initial quarks ejected from $j = 1$, $j = 2$, and $j = 3$ CBCs increases with j, as in the plateau regions the initial quarks carry the increasing momentum fractions $0 \leqslant X \leqslant 1$, $1 \leqslant X \leqslant 2$, and $2 \leqslant X \leqslant 3$, respectively. Furthermore, as the initial quark shares its energy with produced hadrons (antiprotons and nucleons in our case, to satisfy the baryon number conservation), the value of X calculated from Eq. (2) using the kinematical parameters of detected antiprotons turns out to be less than the Bjorken scaling variable x_B in the inclusive electron scattering off nuclei [10,11] when the struck quark absorbs all the energy of the virtual photon. For this reason, the plateaus observed in cumulative antiproton production are shifted toward lower X compared to those in Refs. [10,11].

TABLE VII. Antiproton formation length L in the region where CBCs with $j = 3$ dominate.

$P_{\bar{p}}$ (GeV/c)	1.72	1.53	0.92	0.74	0.66	0.60	0.58
$\theta_{\bar{p}}$ (deg)	59	59	97	97	119	97	119
L(Cu/Be) (fm)	$4.4^{+1.6}_{-1.5}$	$4.4^{+1.8}_{-1.7}$	$4.7^{+1.7}_{-1.8}$	$4.9^{+1.8}_{-1.7}$	$4.9^{+1.6}_{-1.4}$	$4.9^{+1.8}_{-1.7}$	$5.0^{+1.6}_{-1.8}$
L(Ta/Be) (fm)		$4.0^{+1.6}_{-2.5}$	$4.2^{+1.5}_{-2.4}$	$4.3^{+1.6}_{-2.5}$	$4.2^{+1.5}_{-2.4}$	$4.2^{+1.5}_{-2.4}$	$4.4^{+1.5}_{-2.4}$

π^--meson production cross sections, measured in the present experiment at laboratory angles of 10° and 59° simultaneously with antiprotons, were mostly obtained in the kinematically allowed region $X \leqslant 1$. Study of the cumulative pion production by 10-GeV protons in the same set of nuclear targets in the range $1 \leqslant X \leqslant 3.4$ was carried out in our previous work [16]. Similarly to the antiproton case, the ratios $R_j(A/\text{Be})$ increase with an increase in X, but clear plateaus in $R(X)$ were not observed. Note that the model in Ref. [25] implies a flavor-dependent formation length. Contrary to a pion, an antiproton cannot be formed by a valence quark picking up an antiquark from the string breakup. An antiproton can only be created from new $q\bar{q}$ pairs formed inside color strings with a reduced energy resulting from the breakup of the initial string. The string length gets shorter after each break, thus delaying the next pair production [28]. Formation of a $q\bar{q}$ state, i.e., a pion, takes less time than formation of a $3\bar{q}$ state, i.e., an antiproton. Therefore, one can expect a shorter formation length for a pion than for an antiproton under similar initial conditions. Within our simplified model, this results in significant elongation of the second (propagation) stage for cumulative pions and, hence, in an increase in the role of the pion FSIs. These interactions may distort the observed pion spectra and mask the plateaus.

A widely used phenomenological description of antiproton absorption in nuclei boils down to determination of the effective antiproton-nucleon cross section in nuclear matter. Our calculations within the model accounting for both one- and two-step elementary antiproton production processes show that this cross section lies within the range of 40–20 mb at antiproton momenta of 0.6–2.5 GeV/c, which is essentially less than the free inelastic antiproton-nucleon cross section of 100–50 mb at the same momenta [27]. This result is consistent with the findings of an experiment [29] where strong suppression of the annihilation of antiprotons within nuclei was observed in proton-nucleus collisions at a beam energy of 14–17 GeV.

IV. SUMMARY

Inclusive antiproton and π^--meson production cross sections were measured at laboratory angles of 10.5° and 59° and in the momentum range from 0.6 to 2.5 GeV/c during interactions of 10-GeV protons with Be, Al, Cu, and Ta nuclei. Analysis of the antiproton creation cross-section ratios in the region of cumulative variable X ranging from 0.5 to 2.8 was performed. It accounted both for the data obtained in the present experiment and those previously obtained by us for the same set of nuclear targets under laboratory angles of 96° and 119° and with the same initial proton energy.

It was shown that the A dependence of the cumulative antiproton production cross sections is enhanced with an increase in X and is mainly determined by the ratio of the probabilities of the existence of CBCs with $j = 1, 2, 3$ in nuclei with different mass numbers A. In regions where the given CBC dominates, the cross-section ratios demonstrate the presence of three plateaus. In the region of each plateau these ratios exhibit scaling behavior; i.e., they do not depend either on X or on P_t^2. Observation of the plateau in $A(p, \bar{p})$ and in $A(e, e')$ reactions [10,11] in the kinematically forbidden region is indicative of the presence of compact baryon configurations in nuclei—objects of nuclear structure existing at small-distance scales. It was found that the magnitudes of the ratios $R_j(A_1/A_2)$ measured in the $A(p, \bar{p})$ reaction are comparable with those observed in the $A(e, e')$ reaction, which provides evidence of weak absorption of cumulative antiprotons in the nuclear medium. In regions where the contribution to the antiproton production cross section from CBCs with $j = 1, 2, 3$ dominates, the antiproton formation length L increases with an increase in j and reaches a value of 4.5 fm for $j = 3$, which is commensurable with the radius of the Cu nucleus.

Study of cumulative hadron production in proton-induced nuclear reactions provides new information on the features of the hadronization process in cold nuclear medium and may also aid the interpretation of an observable such as jet quenching in hot medium, which was found at the Relativistic Heavy-Ion Collider in high-energy heavy-ion collisions [30] and will be studied at much higher energies at the Large Hadron Collider.

ACKNOWLEDGMENTS

The authors gratefully acknowledge stimulating discussions with A. B. Kaidalov and O. V. Kancheli.

[1] M. M. Sargsian *et al.*, J. Phys. G **29**, R1 (2003).
[2] S. V. Boyarinov *et al.*, Yad. Fiz. **50**, 1605 (1989) [Sov. J. Nucl. Phys. **50**, 996 (1989)].
[3] A. V. Efremov *et al.*, Yad. Fiz. **57**, 932 (1994) [Phys. Atom. Nucl. **57**, 874 (1994)].
[4] L. L. Frankfurt and M. I. Strikman, Phys. Rep. **76**, 215 (1991); **160**, 235 (1998).
[5] C. Ciofi degli Atti and S. Simula, Phys. Rev. C **53**, 1689 (1996).
[6] G. Berlad, A. Dar, and G. Eilam, Phys. Rev. D **22**, 1547 (1980).
[7] M. A. Braun and V. V. Vechernin, Nucl. Phys. B **427**, 614 (1994).
[8] H. J. Pirner and J. P. Vary, Nucl. Phys. A **358**, 413c (1981).
[9] D. B. Day *et al.*, Phys. Rev. Lett. **59**, 427 (1987).
[10] K. Egiyan *et al.*, Phys. Rev. C **68**, 014313 (2003); Phys. Rev. Lett. **96**, 082501 (2006).

[11] N. Fomin, arXiv:0812.2144v1.
[12] J. Aubert *et al.*, Phys. Lett. B **123**, 275 (1983).
[13] J. Gomez *et al.*, Phys. Rev. D **49**, 4348 (1994).
[14] J. Seely *et al.*, Phys. Rev. Lett. **103**, 202301 (2009).
[15] L.B. Weinstein, E. Piasetzky, D. W. Higinbotham, J. Gomez, O. Hen, and R. Shneor, Phys. Rev. Lett. **106**, 052301 (2011).
[16] S. V. Boyarinov *et al.*, Yad. Fiz. **57**, 1452 (1994) [Phys. Atom. Nucl. **57**, 1379 (1994)]; Yad. Fiz. **54**, 119 (1991) [Sov. J. Nucl. Phys. **54**, 71 (1991)]; Yad. Fiz. **56N1**, 125 (1993) [Phys. Atom. Nucl. **56**, 72 (1993)].
[17] M. Sato, S. A. Coon, H. J. Pirner, and J. P. Vary, Phys. Rev. C **33**, 1062 (1986).
[18] J. W. Cronin *et al.*, Phys. Rev. D **11**, 3105 (1975); C. Bromberg *et al.*, Phys. Rev. Lett. **42**, 1202 (1979).
[19] S. Leupold, V. Metag, and U. Mosel, Int. J. Mod. Phys. E **19**, 147 (2010).
[20] Y. Sugaya *et al.*, Nucl. Phys. A **634**, 115 (1998).
[21] T. Ishikawa *et al.*, Phys. Lett. B **608**, 215 (2005).
[22] A. Polyanskiy *et al.*, Phys. Lett. B **695**, 74 (2011).
[23] M. Kotulla *et al.*, Phys. Rev. Lett. **100**, 192302 (2009).
[24] B. Z. Kopeliovich *et al.*, Nucl. Phys. A **782**, 224c (2007).
[25] S. Domdey *et al.*, Nucl. Phys. A **825**, 200 (2009).
[26] W. K. Brooks *et al.*, J. Phys. Conf. Ser. **299**, 012011, (2011).
[27] L. Montanet *et al.*, Phys. Rev. D **50**, 1173 (1994).
[28] B. Kopeliovich and A. H. Rezaeian, Int. J. Mod. Phys. E **18**, 1629 (2009).
[29] I. Chemakin *et al.*, Phys. Rev. C **64**, 064908 (2001).
[30] J. Adams *et al.*, Phys. Rev. Lett. **91**, 172302 (2003); S. S. Adler *et al.*, Phys. Rev. C **69**, 034910 (2004).